Tropical ocean forcing of the persistent North American west coast ridge of winter 2013/14

Richard Seager* and Naomi Henderson

Lamont Doherty Earth Observatory of Columbia University, Palisades, New York

* *Corresponding author address:* Richard Seager, Lamont Doherty Earth Observatory of Columbia University, 61 Route 9W., Palisades, NY 10964. Email: seager@ldeo.columbia.edu

To be submitted to *J. Climate* February 2016, LDEO Contribution Number xxxx.

ABSTRACT

The causes of the high pressure ridge at the North American west coast during winter 2013/14, the driest winter of the recent California drought, are examined. The ridge was part of an atmosphere-ocean state that included atmospheric circulation anomalies across the northern hemisphere and with warm sea surface temperature (SST) anomalies in the tropical west and northeast Pacific and the south Indian Ocean and cool SST anomalies in the central tropical Pacific. The SST anomalies differ sufficiently between data sets that, when used to force an atmosphere model, the resulting simulation of circulation anomalies vary in realism to a striking degree. Recognizing uncertainty in the SST anomalies, we use a series of idealized tropical SST anomaly experiments to identify an optimal combination of SST anomalies that forces a circulation response that best matches observations. The resulting optimal SST pattern resembles that observed. The equilibrium and transient upper troposphere vorticity balance is analyzed to understand the sequence of events that connect these SST anomalies to the west coast ridge. The ridge arose as a summed effect of Rossby waves forced by the collection of SST anomalies with the vorticity balance dominated by relative and planetary vorticity advection terms that drive vortex compression and subsidence at the west coast. The ridge also, in observations and model, shields the west coast from storms which are diverted north and south. The results suggest that tropical Pacific and Indian Ocean SSTs were a key driver of the west coast ridge and drought of winter 2013/14.

1. Introduction

California experienced four consecutive drier than normal winters from 2011/12 to 2014/15 which pushed the state into a record multiyear drought that has had serious social, economic, environmental and agricultural consequences (Howitt et al. 2014). Although intensified by long term warming and coincident high temperatures (Williams et al. 2015), the root cause of the drought has been anomalous high pressure at the west coast of North America which has gone along with fewer than normal winter storms bringing precipitation to California (Herring et al. 2014; Swain et al. 2014; Wang and Schubert 2014; Funk et al. 2014; Hartmann 2015; Seager et al. 2015). In an analysis of ensembles of SST-forced simulations conducted with seven atmosphere models by 5 institutions, Seager et al. (2015) provided evidence that in each of the 2011/12, 2012/13 and 2013/14 winters the west coast ridge and decreased precipitation were importantly, though not entirely, forced by global sea surface temperature (SST) anomalies. Winter 2011/12 was a La Niña event and hence the anomalous high pressure over the northeast Pacific and dry conditions in southwest North America were akin to the canonical response to La Niña events as in Seager et al. (2014a). Winters 2012/13 and 2013/14 were different and formally El Niño- Southern Oscillation (ENSO)-neutral. Despite this, the SST-forced models still tended to produce a west coast ridge and dry conditions at the coast, including California. Seager et al. (2015) argue that the forcing for the ridge originated from the tropical oceans and was a mode of SST-forced variability, albeit one that explained less variance than ENSO or Pacific decadal variability. The SST-forced mode they identified had the west coast ridge associated with an increased SST gradient across the Pacific Ocean with warm anomalies in the western equatorial Pacific and weak cool anomalies in the central to eastern equatorial Pacific. This SST pattern seemed capable of exciting waves that propagated northeast to place the ridge at the North American west coast.

Since the winter of 2013/14 considerable work has been done to try to explain the causes of the unusual weather across the northern hemisphere. Hartmann (2015) came to a similar conclusion as Seager et al. (2015) based on observational and model analysis and Davies (2015) also did via a potential vorticity analysis of transient weather systems. Lee et al. (2015) showed that many features of the observed circulation anomaly could be reproduced within an atmosphere model forced by the SST and sea ice anomalies that prevailed during the winter arguing for roles for tropical, extratropical and subpolar forcing. On the other hand Baxter and Nigam (2015) showed how the observed circulation anomalies could be understood in terms of known patterns of variability such as the West Pacific-North Pacific Ocean mode and argued for an origin in terms of internal mid-latitude variability. They criticized Seager et al. (2014c) for "succumbing to the post 1980s-90s temptation" of ascribing Pacific-North America variability to tropical sources and, together with Hartmann (2015), for failing to provide "process-level observational support" via, for example, analysis of outgoing longwave radiation or diabatic heating. Succumbing to temptation is not always a bad move and can lead to positive outcomes. Watson et al. (2015) in a modeling and observational study, showed that the warm SST anomalies in the tropical west Pacific Ocean did indeed correspond to positive precipitation anomalies (and therefore diabatic heating) and showed that this was one, but by no means the only, process at play in generating the west coast ridge of winter 2013/14.

The work performed to date has pointed to answers in regard to generation of the west coast ridge that forced the California drought but leaves many questions unanswered. The current work extends beyond the prior work in terms of examining the physical processes involved in generating the ridge. For example, one leading question is: if we accept a role for ocean forcing, which we do, where is it in the global ocean that the forcing for the ridge originates and is one region with a simple wave response (e.g. the tropical west Pacific) or multiple regions with superimposed or interacting waves responsible? What were the anomalies in the precipitation-bearing North Pacific storm track associated with the ridge? What are the physical mechanisms of wave-mean flow-transient eddy interaction that connect the SST anomalies to the west coast ridge and suppression of precipitation? Further, once the culprit ocean state has been identified, what ocean-atmosphere processes were responsible for creating that state? Here we will address the first two questions and leave the third oceanographic question aside while noting that for the general problem of drought far less attention is paid to the causes of the responsible SST anomalies than to the atmospheric response to them.

Here we report on a series of modeling experiments designed to understand the non-ENSO ocean forcing of the west coast ridge focusing in on winter 2013/14 as the more extreme of the two years that had this feature. It is found here that the usual methodology of imposing actual SST anomalies by ocean basin and region in order to locate the prime forcing region for the response feature of interest does not work well for the case of winter 2013/14. Reasons for this are discussed and in part relate to uncertainties in the SST field itself that may have effected the model-based analyses by the prior workers mentioned above. Recognizing this we turn to a series of idealized SST forcing experiments and use an optimization procedure to identify the combination of tropical SST and associated diabatic heating forcing that leads to the best match for the observed circulation anomaly. The implied SST and precipitation anomalies are compared to those observed and linearity is assessed by rerunning the model forced by the optimal SST forcing pattern. The modeling experiments implicate a collection of SST anomalies in the Indian and tropical Pacific Oceans as combining to help force the west coast ridge and drought of winter 2013./14. We then study the observed and modeled upper troposphere vorticity balance to understand the physical mechanisms that underlay the persistent west coast ridge. To complete the study we then analyze the transient day-by-day and week-by-week adjustment of the atmospheric circulation and vorticity balance in response to the switch-on of the optimal SST forcing field, allowing cause and effect to be successfully diagnosed.

2. Observational data and model simulations

a. Observations

For anomalies in the atmospheric circulation during winter 2013/14 we use the National Centers for Environmental Prediction-National Center for Atmospheric Research (NCEP-NCAR) Reanalysis (Kistler et al. 2001) accessed via the International Research Institute for Climate and Society Data Library at `http://iridl.ldeo.columbia.edu/expert/SOURCES/.NOAA/.NCEP-NCAR/.CDAS-1/.MONTHLY/`. To analyze global precipitation we use the satellite-gauge data from the Global Precipitation Climatology Project (GPCP) (Adler et al. 2003) also accessed from the IRI Data Library at `http://iridl.ldeo.columbia.edu/`

SOURCES/.NASA/.GPCP/.V2p2/.satellite-gauge/. For SST we analyzed the Hadley Center HadISST data product (Rayner et al. (2003), accessed from http://www.metoffice.gov.uk/hadobs/hadisst/data/download.html), the National Oceanic and Atmospheric Administration (NOAA) Extended Reconstructed SST version 4 data (ERSSTv4, Huang et al. (2015), accessed from http://iridl.ldeo.columbia.edu/SOURCES/.NOAA/.NCDC/.ERSST/.version4/) and the European Centre for Medium Range Weather Forecasts (ECMWF) Ocean Reanalysis (ORAs4) of Balmaseda et al. (2013) accessed from https://reanalyses.org/ocean/overview-current-reanalyses. Surface latent and sensible heat flux data are from Yu et al. (2008), accessed from http://oaflux.whoi.edu/data.html, and make use of surface and satellite information and are referred to here as the OA fluxes.

The atmosphere model we use is the NCAR Community Climate Model 3 (CCM3, Kiehl et al. (1998)). CCM3 is a vintage model but has been the workhorse model at Lamont for over a decade. It was used for the 16 member, 1856 to current, SST-forced ensembles, the analysis of which have led to considerable advances in understanding North and South American drought history (Seager et al. 2005, 2009, 2010a) and has also been applied to understanding the evolution of transient eddy-mean flow interaction over the Pacific-North America region during ENSO events (Seager et al. 2010b). 16 member, 1856 to recent, ensembles with more recent NCAR models, Community Atmosphere Models (CAMs) 3, 4 and 5, have also been generated at Lamont and compared to CCM3. By standard measures - pattern correlations between modeled and observed precipitation or between modeled soil moisture and observationally-based Palmer Drought Severity Index across North America, time series correlations between these quantities for key regions - CCM3 performs as well as, and usually much better than, the CAM models (see the comparison at http://rainbow.ldeo.columbia.edu/~jennie/comparemodel/). Since CCM3 also uses about one fifth the computing time of the CAMs, allowing for large ensembles and numerous experiments, we will use the vintage CCM3 once more here.

We conduct two types of modeling experiment:

i. 100 member ensembles forced by historical observed SST anomalies during December 2013 to February 2014 were generated using different SST data sets as forcing. The ensemble mean is analyzed as an anomaly relative to the January 1979 to April 2014 climatology of a 16 member ensemble forced with Hadley Centre SSTs. The 100 ensemble members are initialized on December 1 2013 with different initial conditions taken from December 1 atmospheric and land surface states of long model simulations with repeating climatological SSTs.

ii. 100 member ensembles simulating the 100 days beginning December 1 in which fixed idealized SST anomalies are added to the Hadley Centre SST climatology. An additional 100 member ensemble was generated using the same initial conditions but climatological SSTs. The ensemble mean of the differences between the 100 perturbed and control pairs was then analyzed at daily and time-averaged temporal scales. The perturbed simulations are forced by "box-SST anomalies" centered on the Equator at different longitudes from the Indian Ocean to the eastern tropical Pacific. Each anomaly has a maximum of $1°C$ and is in a box centered on the Equator stretching from $10°S$ to $10°N$ and spanning 30° in longitude with smoothing to zero anomaly at the edges. Experiments were run for both warm and cold SST anomalies with results shown for the warm minus cold experiments divided by two.

3. Atmosphere-ocean conditions during winter 2013/14

We focus on the winter of 2013/14 which was the driest, as measured by all-California, November through April precipitation reduction, so far in the current California drought (Seager et al. 2015). We also focus on the December through February (DJF) season at the heart of winter.

Figure 1 shows the observed 200mb height anomaly, the GPCP precipitation anomaly, the ERSSTv4 SST anomaly, and the latent plus sensible OA flux anomaly for DJF 2013/14 all relative to a January 1979 to April 2014 climatology. The height anomaly includes a north-northwest to south-southeast oriented ridge immediately west of the North American coast and extending from Alaska to Mexico. The ridge is part of a more general area of high geopotential heights that extends west over the North Pacific, Bering Sea and eastern Siberia. There was also a deep trough centered over Hudson Bay, responsible for the very cold winter in northeast North America (Hartmann 2015; Baxter and Nigam 2015), low heights over the mid-latitude North Atlantic and high heights over the subtropical North Atlantic (although not with the canonical positive North Atlantic Oscillation pattern).

The precipitation anomaly associated with this height pattern shows the dry conditions along the U.S. west coast and expanding into British Columbia, northwest Mexico and the central U.S. The west coast and central North America dry anomalies are under northerly (and presumably subsiding) upper level flow. Over the North Pacific, wet anomalies occur on the western, southerly, flowing flank of the ridge and another dry anomaly under northerly flow over the northwest Pacific. In the tropics there was a dry anomaly over the central to eastern Pacific, a wet anomaly northwest of Papua New Guinea, generally neutral to dry conditions over the maritime continent and wet conditions over the Indian ocean just south of the Equator.

The SST anomaly (contours in the middle panel of Figure 1, colors in Figure 2) shows a broad region of warm anomalies in the Indian Ocean centered south of the Equator and in the western tropical Pacific, cool anomalies in the central to eastern tropical Pacific and a remarkably warm anomaly in the northeast Pacific south of Alaska and west of British Columbia and Washington State. The colors in the lower panel of Figure 1 are the surface latent plus sensible heat flux, defined here as positive into the ocean. Notably the warm North Pacific SST anomalies are associated with anomalous flux of heat into the ocean, i.e. atmospheric forcing of the anomalies. Further, Bond et al. (2015) performed an ocean mixed layer heat budget analysis of the northeast Pacific warm anomaly and found the prime driver of it was a reduction in entrainment of cool water into the mixed layer as a consequence of extreme low wind speeds. Hence, via both surface fluxes and mixed layer processes, the northeast Pacific warm anomaly appears a result of the west coast ridge and not a driver. In contrast, the warm SST anomaly in the tropical west Pacific was associated with an anomalous flux of latent plus sensible heat from the ocean to the atmosphere. There is also a region on the Equator at the dateline of anomalous ocean heat uptake. This corresponds to a region of negative precipitation anomaly in the GPCP data but is at the border between positive and negative SST anomalies in the ERSSTv4 analysis.

These associations are suggestive of ocean driving of the atmosphere in the tropics and the opposite over the North Pacific, an entirely familiar state of affairs in interannual climate variability that has been well known dating back to Alexander (1992a,b), Cayan (1992) and Lau and Nath (1994, 1996). However, it should be noted that what the SST anomaly was during DJF 2013/14 is not clear. Figure 2 (left column) shows maps for the anomaly, all relative to the same 1979 to 2014 climatology, for the Hadley, ORAs4 and ERSSTv4 data sets. All three disagree on the amplitudes of the warm SST anomalies in the North Pacific and in the tropical west Pacific and the cold anomaly in the central equatorial Pacific Ocean. Some of this disagreement is to be expected since the ERSSTv4 data set only uses in situ measurements while Hadley and ORAs4 also use satellite data (but with different sources for the latter) and the analysis methods used to obtain gridded data sets differ.

As seen in the reanalysis-based moisture budget analysis of Seager et al. (2014c), precipitation at the west coast of North America arises from the combined effect of mean westerly winds and orographic uplift at the coast and the propagation onshore from the west of storm systems within the Pacific storm track. Hence, the west coast ridge of winter 2013/14 is partly directly responsible for the dry conditions along the west coast of the U.S. by weakening the prevailing westerlies. However, Seager et al. (2014c) also show that moisture convergence by transient eddies is very important, especially for there being precipitation in southern California and northern Mexico in winter. A measure of the storm track activity is the high-pass filtered upper tropospheric meridional velocity variance. Using daily data from the NCEP Reanalysis we computed this using a fourth order Butterworth filter with a 10 day cutoff and the lower panel of Figure 1 shows the anomaly for DJF 2013/14. There was a rather striking banded structure across the eastern North Pacific and North America with reduced eddy activity centered around the latitude of California and increased activity to the north. This implies fewer and/or weaker storms entering the southern portions of the west coast and, along with the mean high pressure ridge, is consistent with reduced precipitation (and the California drought).

The differences in the SST anomalies matter for the atmospheric response. Figure 2 (right column) shows the modeled ensemble mean 200mb height and precipitation response to the DJF 2013/14 global SST anomalies when the Hadley, ORAs4 and ERSSTv4 versions are added to the same climatological SST. All three SST anomaly patterns force high height anomalies at the west coast but with Hadley and ORAs4 having a more realistic elongated northwest to southeast orientation. ORAs4 SST forcing also produces a Hudson Bay trough. The associated precipitation anomalies also largely agree with the observations with dry across the central to eastern tropical Pacific, wet over the western tropical Pacific. However, with Hadley SST forcing, the western tropical Pacific wet anomaly is split in two by a westward extension of the equatorial Pacific dry zone. The model simulations all agree on wet conditions over the southern Indian Ocean and dry to the north which is clearly a simple response to the warm-cold south-north Indian Ocean SST anomalies but which is only hinted at in the GPCP observed precipitation anomaly.

Despite the noted aspects of model-observations agreement, all three forced responses differ from the observations and are much weaker, as expected if the observed anomaly combined an SST-forced response with internal atmospheric variability. Also all three forced responses differ. This is despite the experiments being done with the same model and with the anomalies being imposed on the same SST climatology and the ensemble containing 100 members which highly effectively isolates the forced response. The message is that clearly the differences in SST anomalies between the different data sets matter and, of course, we cannot tell easily which SST data set is more accurate. It is sobering to realize that, in this important case, modern observations and analysis methods cannot constrain SST anomalies to the accuracy required to successfully model the atmospheric response.

An additional problem with SST-forced experiments for winter 2013/14 concerns the North Pacific warm SST anomaly. In experiments we have performed with SST forcing restricted to the tropics only and the North Pacific only, it is clear that the response to global SSTs seen in Figure 2 involves both. However, when the North Pacific SST anomaly is imposed alone the atmosphere model responds by increased ocean to atmosphere surface heat flux, northerly winds above (which can balance the heating with advective cooling as in Hoskins and Karoly (1981)) and a high to the west. This response is essentially the opposite of the flow-flux relationship seen in observations during DJF 2013/14 (Figure 1 and (Bond et al. 2015)) and is consistent with being a spurious model response to an imposed SST anomaly that was in fact generated by the atmospheric flow pattern. All of the simulated responses in Figure 2 will be corrupted by some element of this spurious response.

4. Constructive modeling of the west coast ridge of winter 2013/14

The above results and arguments make clear that we cannot expect to explain the origin of the circulation anomalies of DJF 2013/14 by simply imposing an "observed" SST anomaly as the lower boundary condition for an atmosphere model. Instead we will adopt a more roundabout route that seeks to identify a combination of idealized SST and associated diabatic heating anomalies that can reproduce the circulation anomaly.

a. "Box-SST anomaly" experiments

Turning to the results of the "box-SST anomaly" modeling experiments, we begin by noting that the circulation of DJF 2013/14 is unlike any familiar wave trains produced by these localized SST anomalies. Figure 3 shows the 200mb geopotential height anomaly responses (right column) to the imposed box SST anomalies (left column). A warm SST anomaly in the central equatorial Pacific Ocean forces a single wave train that is quite characteristic of El Niño events with a low height anomaly over the North Pacific and a high anomaly centered over western Canada. The same size SST anomaly to the east is less effective at forcing a response in the height field. As the warm anomaly is moved west the response moves west too but also weakens and then changes character when the warm SST box is placed in the Indian Ocean. In that case a rather zonally symmetric response results with low height anomalies over northern Canada and high height anomalies over the North Pacific and North Atlantic, somewhat reminiscent of the warm Indian Ocean-positive North Atlantic Oscillation connection identified by Hoerling et al. (2001). Clearly the observed DJF 2013/14 height anomaly is not very akin to any of these patterns, or their opposite.

b. Optimal combinations of "box-SST anomaly" responses that match DJF 2013/14

Given that the circulation of DJF 2013/14 cannot be easily explained as a response to a localized SST anomaly can it be explained as a combination of wave responses to a variety of SST anomalies and, if so, can this be understood in terms of linear superposition of the different waves? To assess this we seek the optimal linear combination of "box-SST anomaly" response patterns that best matches the observed DJF 2013/14 200mb height anomaly for all longitudes and from $25°N$ to $75°N$. This map, Z'_{NCEP}, is our target pattern and is a subset of the field shown in Figure 1.

We denote the 200mb heights from the box-SST anomaly experiments as Z_j. We use a constrained linear least squares optimization to find the best approximation of the Z'_{NCEP} using linear combinations of the Z'_j with the constraint that the SST anomalies are less than $1K$. This can be expressed as the problem of finding N constants, c_j, which achieve the distance minimization:

$$\min_{\mathbf{c}} \left(\| \sum_{j=1}^{N} c_j Z'_j(\mathbf{x}) - Z'_{NCEP}(\mathbf{x}) \| \right) \tag{1}$$

subject to the constraint:

$$|c_j| \leq 1, \tag{2}$$

where the global area-weighted energy norm over all gridpoints $\mathbf{x} = (\lambda, \phi)$, where λ is longitude and ϕ is latitude, is

$$\|f(\mathbf{x})\|^2 \equiv \frac{\sum_{\mathbf{x}} f^2(\mathbf{x}) \cos(\phi)}{\sum_{\mathbf{x}} \cos(\phi)}.$$

Finding the c_j for $j = 1$ to 5 from the above procedure produces the 200mb height anomaly pattern shown in Figure 4. The optimization is able to create a west coast-North Pacific ridge and also a weak Hudson Bay trough pattern that, though far from a perfect match, is clearly related to that observed. The optimized pattern is also weaker than that observed. The differences in structure and amplitude are not necessarily a problem if the observed pattern combines an SST-forced response with constructive internal atmosphere variability. Figure 4 also shows the corresponding SST and precipitation anomalies, derived from the same linear combination of "box-SST anomaly" experiments. The optimization suggests the circulation anomaly arose as a response to a collection of SST anomalies and associated precipitation anomalies. The best match requires a modestly warm eastern Indian Ocean, near normal over the Maritime Continent region, warm in the western tropical Pacific Ocean and cool across the central and eastern tropical Pacific Ocean. The precipitation anomalies the model produces closely match the SST anomalies in a warm-wet, cool-dry sense as expected, and also have some similarity to the observed precipitation anomalies in Figure 1. It is noteworthy that, out of all the possible combinations of sign and amplitude and location of SST anomalies that the optimization could have chosen to find a response field that best matches the observed height field, it chose one that has a clear resemblance to reality.

c. Checking for linearity of the response to collections of SST anomalies

Identifying a linear combination of "box-SST anomaly" responses that best matches the observed circulation does not mean that, if forced with the associated linear combination of SST anomalies, the atmosphere model would reproduce the same circulation. This is because the model is nonlinear and allows for the possibility that the waves forced from the various ocean regions will interact with each other to produce a response that departs from the linear assumption. To check this we forced the atmosphere model with the optimal linear combination SST pattern and the results are shown in the lower panel of Figure 4. The model 200mb height response to the optimized SST anomalies is very similar in the important details to the optimal sum of the individual box experiments, confirming the essential linearity of the response. That is, the total response can be understood as the linear combination of waves forced by the components of the total SST anomaly field with little important interaction between the forced waves.

5. Tropical Indo-Pacific SST anomaly forcing of circulation and storm track anomalies in the eastern North Pacific and North America sector

Tropical SST anomalies can exert a strong influence on the strength and latitude of the Pacific storm track over the eastern North Pacific and west coast of North America. Returning to the "box-SST anomaly" experiments, Figure 5 shows the ensemble mean change in the 200mb high pass filtered meridional velocity variance averaged over days 40-100 of each experiment. Depending on where the SST anomaly is located it can have quite different effects on the Pacific storm track. For a warm SST anomaly in the central equatorial Pacific a rather classic El Niño-like southward displacement and strengthening of the storm track from the central North Pacific to North America occurs as analyzed in detail in Seager et al. (2010b) and Harnik et al. (2010). The argument in those papers is that the storm track displacement occurs as the transient eddies are refracted more equatorward as a consequence of strengthened subtropical westerly winds that occur poleward of the diabatic deep convective heating anomaly generated by the warm SST anomaly. A warm SST anomaly in the far western tropical Pacific generates a similar but weaker southward storm track displacement. In contrast a warm SST anomaly in the maritime continent region induces only a weak response while one over the Indian Ocean cause a strong poleward displacement with increased eddy activity over British Columbia and Alaska and decreased activity over California and Mexico.

Returning to Figure 1 (lower panel), it is seen that winter 2013/14 had a reduction of eddy activity centered over the eastern North Pacific and North America at the latitude of California with increased activity over southwestern Canada and over the subtropical eastern North Pacific. From Figure 5, this would appear to be a pattern that could be induced by a combination of tropical SST anomalies, including a warm anomaly over the western tropical Pacific, which can cause a reduction of eddy activity at the location of California and an increase over the subtropical North Pacific Ocean to the south of there.

Figure 6 shows the evolution of the mean and transient circulation response in the model forced by the switch-on of the optimized SST anomaly pattern. Here the ensemble mean anomaly will, over the 10-15 day time period of initial value predictability when the ensemble members closely resemble each other, represent the daily evolution of the forced response to the imposed SST anomaly. After that, the ensemble members will diverge and time averaging is needed to identify more closely the SST-forced response. Hence in Figure 6 we begin by showing daily values and then move on to showing time averages. The initial response involves positive height anomalies straddling the equator over the west Pacific Ocean: a classic Gill (1980) response to increased convection and vertical motion above warm SST anomalies. A few days later this tropical source has been joined by others, including weaker highs over the Indian Ocean and lows over the cool waters of the central equatorial Pacific. A few days later these sources have already triggered well developed wave trains with a high anomaly at the west coast of North America that intensifies over the subsequent week. It is clear the mean circulation response is not comprised of a single source-plus-wave response but combines multiple sources and forced responses. In tandem with the wave trains, the weaker eddy activity over the midlatitude eastern North Pacific Ocean and the United States and Mexico begins to be established by day 8 and also intensifies with the height anomalies over the subsequent week. The eddy weakening occurs where there are local easterly anomalies at 200mb and the strengthening where anomalies are westward. This relation is consistent with changes in transient eddy propagation paths responding to the changes in the mean flow as in Seager et al. (2010b).

6. The dynamical balance within the mean and transient circulation anomalies of winter 2013/14

a. The quasi-equilibrium vorticity balance in Reanalysis and model simulation

How did the atmosphere achieve a statistical steady state during winter 2013/14 that included such strong departures from the normal state? To examine this we turn to the upper troposphere vorticity budget which can be written as:

$$\frac{\partial \hat{\zeta}}{\partial t} + \hat{\mathbf{u}} \cdot \nabla \hat{\zeta} + \beta \hat{v} = -(\hat{\zeta} + f) \nabla \cdot \hat{\mathbf{u}} - \nabla \cdot \widehat{(\mathbf{u}'' \zeta'')} + \hat{F}, \tag{3}$$

where the hats denote monthly means and the double primes departures therefrom, ζ is relative vorticity, $\mathbf{u}$ is the horizontal vector velocity, f is the Coriolis parameter and β its meridional gradient, v is meridional velocity, F includes friction, diffusion and the residual imbalance and t is time. Terms involving vertical advection of vorticity, which tend to be small, have been neglected.

A common way to diagnose forcing of Rossby waves by tropical heating anomalies is to separate the anomalous flow into its rotational, denoted by subscript ψ, and divergence, denoted by subscript χ, components, i.e. $\hat{\mathbf{u}} = \hat{\mathbf{u}}_\psi + \hat{\mathbf{u}}_\chi$. Using this, and denoting anomalies of monthly means by a single prime and climatological monthly means by an overbar, the anomaly vorticity equation can be rewritten as:

$$\frac{\partial \hat{\zeta}'}{\partial t} + \bar{\hat{\mathbf{u}}}_\psi \cdot \nabla \hat{\zeta}' + \hat{\mathbf{u}}'_\psi \cdot \nabla \bar{\hat{\zeta}} + \beta \hat{v}'_\psi = -(\bar{\hat{\zeta}} + f) \nabla \cdot \hat{\mathbf{u}}'_\chi - \hat{\zeta}' \nabla \cdot \bar{\hat{\mathbf{u}}}_\chi - \beta \hat{v}'_\chi - \bar{\hat{\mathbf{u}}}_\chi \cdot \nabla \hat{\zeta}' - \hat{\mathbf{u}}'_\chi \cdot \nabla \bar{\hat{\zeta}} - \nabla \cdot \widehat{(\mathbf{u}'' \zeta'')}' + \hat{F}'. \tag{4}$$

These terms were computed for the observations from the NCEP-NCAR Reanalysis averaged over DJF 2013/14 with anomalies defined as relative to a 1979 to 2014 climatology. The right hand side, minus the damping term, is referred to as the Rossby Wave Source (RWS) (Sardeshmukh and Hoskins 1988; Trenberth et al. 1998). Watson et al. (2015) show the RWS from ECMWF analysis for the west Pacific domain and separate it into divergent and advection terms. The RWS appears qualitatively similar to those shown here from NCEP-NCAR but we continue by breaking the term down into its constituent parts to afford a more detailed process understanding. It was found that $\partial \hat{\zeta}'/\partial t$, $\hat{\zeta}' \nabla \cdot \bar{\hat{\mathbf{u}}}_\chi$, $\bar{\hat{\mathbf{u}}}_\chi \cdot \nabla \hat{\zeta}'$ were sufficiently smaller than the other terms so that they could be neglected in understanding the vorticity balances and its establishment. $\hat{\mathbf{u}}'_\chi \cdot \nabla \bar{\hat{\zeta}}$ is also small but is retained since this term has been appealed to as an important forcing in prior literature. Written in this way the rotational flow, as described by the left hand side, can be understood as a response to forcing involving the divergent flow on the right hand side. The eight larger remaining terms are shown in Figure 7.

The vorticity balance anomalies are seen to occur as part of waves of anomalies that stretch to North America from the Indian and tropical Pacific Ocean regions. Across the east Pacific and North America there is a strong opposing relationship between, on the one hand, advection of planetary vorticity by the rotational meridional wind anomaly $\beta \hat{v}'_\psi$ plus mean flow advection of the vorticity anomalies $\bar{\hat{\mathbf{u}}}_\psi \cdot \nabla \hat{\zeta}'$ and, on the other hand, vortex stretching (represented by $f \nabla \cdot \hat{\mathbf{u}}'_\chi$) with northerly flow and subsidence (not shown) at the west coast of North America. The subsidence would suppress precipitation, consistent with drought conditions. Advection of the vorticity anomalies by the mean flow is dominated by the mean zonal wind term (not shown) and, while being important to setting up the vertical motion, also acts to translate the pattern eastward. In contrast to the balance over the eastern Pacific-North America sector, over the Indian and west Pacific sectors, the advection of the mean relative vorticity by the rotational flow anomalies, dominated by $\hat{v}'\partial\hat{\bar{\zeta}}/\partial y$, is important. This term sets up an east-west varying pattern that reflects the zonal variation in meridional flow anomalies that arises from the circulation responses to the multiple SST and convection anomalies in the tropics. These flow anomalies are located in a region of strong zonally uniform meridional gradient of mean relative vorticity giving rise to this complex pattern.

The mechanism of establishment of the forcing for the Rossby waves differs somewhat from classical thinking (Sardeshmukh and Hoskins 1988; Trenberth et al. 1998) in that, across Asia and the subtropical west Pacific, the advection of mean relative vorticity by the anomalous divergent flow is much smaller than that by the rotational flow. Hence we do not have a clean separation with the rotational flow evolving in response to changes in the divergent flow. Instead the forced rotational flow interacts with the mean flow to cause a further evolution of the rotational flow anomaly.

The vorticity budget terms were also averaged over the last 60 days of the optimal SST-forcing simulations. It was found that the terms that were small in the Reanalysis were also small in the model and the same eight larger terms in the model are shown in Figure 8. The relative importance of the terms in the vorticity budget are very similar between the models and the Reanalysis. The one exception is the much smoother transient eddy vorticity convergence in the model than the Reanalysis which simply comes about from the averaging across a 100 member ensemble compared to Nature's single realization. The individual terms in the vorticity balance also bear some similarity between model and Reanalysis. The model agrees that advection of the mean relative vorticity by the rotational flow dominates over that by the divergent flow. Similarly this sets up in the model a zonally varying, meridionally confined, anomalous vorticity tendency over south Asia and the subtropical west Pacific. The locations of the features within this term, however, do not agree between the model and Reanalysis, which could be due to model bias in the location of the tropical heating, the flow response, or in the mean state which allows a phase error in the wave response. Further, over western North America the model agrees with the observations that the upper troposphere convergence and, hence, subsidence below, arises from a three way balance between vortex stretching, advection of planetary vorticity by the rotational meridional velocity anomaly and advection by the mean flow of the vorticity anomaly.

The transient eddy vorticity flux convergence term is not small. However it also does not appear to systematically contribute to the maintenance of the large scale circulation anomaly pattern being instead rather noisy. This is in contrast to the results of Seager et al. (2003, 2010b) and Harnik et al. (2010) who found that transient eddy momentum fluxes were important to developing and sustaining mean flow anomalies during El Niño events. However the results are not necessarily inconsistent. The earlier results concerned El Niño events which could have a different eddy-mean flow interaction process to that occuring during winter 2013/14 and its model analog. Also the earlier results made much of the case for a positive eddy-mean flow feedback by analyzing longitudinally averaged quantities whereas here our focus is on explaining the west coast ridge of winter 2013/14, a very longitudinally localized feature.

b. The transient evolution of the vorticity balance in the model simulation

It is not possible to establish cause and effect in the establishment of the vorticity balance in the Reanalysis because the atmosphere is always in a statistical equilibrium with the slowly evolving SST anomalies. Hence we return to the model simulations subject to an instantaneous switch on of the SST anomaly and, as we did in Figure 6 for the height field and storm track, examine how the vorticity budget evolves on a day-by-day and weekly basis. Results are shown in Figure 9 for the leading terms in the vorticity budget given by:

$$\hat{\mathbf{u}}'_{\psi} \cdot \nabla \hat{\bar{\zeta}} + \hat{\bar{\mathbf{u}}}_{\psi} \cdot \nabla \hat{\zeta}' + \beta \hat{v}'_{\psi} = -f \nabla \cdot \hat{\mathbf{u}}'_{\chi}. \tag{5}$$

Early on at day 5 there are various vorticity tendency terms related to the advection of the mean relative vorticity gradient by the anomalous rotational flow across the tropical Pacific north of the Equator. This term is dominated by the $\hat{v}'_{\psi}\hat{\bar{\zeta}}_y$ component (not shown). This entire term has grown by day 9 and is being balanced in large part by mean flow advection of the relative vorticity anomaly and to a lesser extent by the term involving the upper troposphere divergence anomaly. The latter term has now established convergence over the west coast of North America that, by mass continuity, will require subsidence below. Further examination shows that, over the west Pacific, the advection of mean relative vorticity by the anomalous rotational flow is dominated by the meridional flow anomaly but in the east Pacific-North America sector the advection by anomalous zonal flow is the leading term. The vorticity balance terms intensify to day 13 but the balance among the terms remains essentially the same.

This can be understood in terms of the transient evolution of the flow anomaly field $(\hat{u}'_{\psi}, \hat{u}'_{\chi}, \hat{v}'_{\psi}, \hat{v}'_{\chi})$ as shown in Figure 10. The warm SST and positive precipitation anomaly over the west Pacific Ocean excites local upper troposphere off-equatorial anticyclonic anomalies to the west and equatorial westerly and cyclonic anomalies to the east. The latter are more clear because the heating forced response to the west is interfered with by responses to the other SST anomalies further west over the Maritime Continent region and Indian Ocean. Looking at the transition from day 5 to day 9, the cyclonic anomaly over the east Pacific is now at the root of a wave train that has propagated northeastward and placed easterly anomalies at the west coasts of the United States and Mexico. In addition a wave that is particularly well expressed in the meridional flow field has propagated from the northern Indian-south Asia-southwest Pacific region eastward across the Pacific and placed northerly flow at the west coast centered on the Canada-U.S. border region. The vorticity balance that is established therefore arises from a combination of these wave fields originating across the Indo-Pacific region but with the end result of high pressure and subsidence at the west coast of North America that would act to suppress precipitation.

7. Conclusions and Discussion

We have investigated the dynamical causes of the North American west coast ridge of winter 2013/14 that caused the driest winter during the recent California drought and sought to relate it to SST anomalies in the tropical Pacific and Indian Oceans. Conclusions are as follows:

- Prior work has linked the drought-inducing North American west coast ridge of winter 2013/14 with SST anomalies. However different SST data sets disagree on the amplitude and to some extent the pattern of the SST anomalies with the result that the same atmosphere model forced by the different SST data sets simulates the ridge with starkly different levels of realism.

- Motivated by the uncertainty in regard to the SST anomalies that were actually present in winter 2013/14, we adopted a "constructive modeling" approach and found an optimal pattern of tropical Indo-Pacific SST anomalies that produced a model response that best matched the observed Northern Hemisphere height anomaly in DJF 2013/14. A pattern with a warm SST anomaly in the west Pacific, cool in the central Pacific, near neutral in the Maritime Continent region and warm again in the Indian Ocean produces a height response that provides the best match including a west coast ridge. The height response can be understood as a linear combination of waves forced by the individual anomalies.

- In both observations for DJF 2013/14 and the optimal forcing simulations the west coast ridge is also associated with suppression of storm track activity with increased activity towards the north and south. This rearrangement of transient eddy activity, which essentially acts to shield California from moisture-laden storms, would have aided in generating drought conditions.

- The fundamental features of the vorticity balance within the circulation anomaly are associated with the mean flow terms involving advection of the mean relative vorticity field by the rotational flow, advection of the relative vorticity anomaly by the mean zonal flow, the anomalous planetary vorticity advection and vortex stretching. It is vortex compression over the west coast that will act to induce subsidence and also suppress precipitation. We do not find clear evidence of a feedback between the eddy vorticity fluxes and the mean flow.

- The transient day-by-day and week-by-week evolution of the model response to the optimal SST forcing shows that the collection of tropical SST anomalies generate upper troposphere rotational flow anomalies that create anomalous advection of mean relative and planetary vorticity and force Rossby waves that propagate and within days reach the west coast of North America establishing the ridge by the vorticity balance described above. As the mean flow circulation anomaly develops so does the reduction in eddy activity over the west Pacific and North America at the latitude of the United States and Mexico.

To conclude, the work presented here is highly suggestive that tropical Indian and Pacific SST anomalies and associated precipitation anomalies forced a collection of Rossby wave responses that in sum provided the unusual North American west coast ridge of winter 2013/14. Hence, we argue, that the ridge depended on a more general anomalous tropical ocean state than just the warm western tropical Pacific whose impacts were focused on by Watson et al. (2015). The results are, however, not conclusive largely because the actual SST anomalies during this winter are not known to the level of accuracy that is apparently needed to successfully reproduce in models the correct atmospheric response. Hence it remains uncertain exactly what SST anomalies were responsible and also whether there was an additional role in the wave forcing for precipitation anomalies that were not tied to the underlying SSTs. A clear avenue for future research must be to determine why different state-of-the-art SST data sets differ to the degree they do in the modern era of quite abundant observational data. A second avenue for research should be determine what caused the drought-forcing SST anomalies. The results indicate that they were driven by anomalous ocean heat flux convergence but the causes of that are unknown. It would be interesting to identify the wind forcing and changes in currents, mixing and thermocline depth responsible and to also determine if these arise as an occasional part of the ENSO cycle or are a different phenomena, or are influenced by human-driven climate change.

The results presented here also do not preclude the possibility that other additional processes were also involved in generating the west coast ridge, including internal atmosphere variability as argued by Seager et al. (2014b), Baxter and Nigam (2015) and Watson et al. (2015) or forcing from other changes in ocean surface conditions (Lee et al. 2015). In terms of any role for climate change it should noted that the current work indicates that a key feature of the SST anomaly for generating the ridge was warming in the west Pacific relative to the more eastern part of the ocean. That is why Palmer (2014) noted that for anthropogenic climate change to have played a role in the SST states that contributed to the extreme winter of 2013/14 it would require a non-uniform SST response to radiative forcing and essentially invoked the ocean dynamical thermostat mechanism of Clement et al.

(1996) and Cane et al. (1997). Whether such a dynamically-influenced forced SST change is occurring in nature is unknown but needs to be determined. Whatever the answer, that tropical SST anomalies that are neither El Niño nor La Niña can help create such a dramatic climate anomaly over North America as the west coast ridge of winter 2013/14 is interesting and, now that it is identified, should provide a means to improve seasonal prediction for the continent provided that the SST anomalies can first be monitored with sufficient accuracy and secondly predicted.

Acknowledgments.

This work was supported by NSF awards AGS-1401400 and AGS-1243204 and NOAA award NA14OAR4310232. We thank Dong-Eun Lee for conversations and some additional simulations analyzing sensitivity of circulation anomalies to SST data sets.

REFERENCES

Adler, R. F., et al., 2003: The version-2 global precipitation climatology project (GPCP) monthly precipitation analysis (1979-present). *J. Hydrometeor.*, **4**, 1147–1167.

Alexander, M. A., 1992a: Midlatitude atmosphere-ocean interaction during El Niño. Part I: The North Pacific Ocean. *J. Climate*, **5**, 944–958.

Alexander, M. A., 1992b: Midlatitude atmosphere-ocean interaction during El Niño. Part II: The northern hemisphere. *J. Climate*, **5**, 959–972.

Balmaseda, M. A., K. Mogensen, and A. T. Weaver, 2013: Evaluation of the ECMWF ocean reanalysis system ORAS4. *Quart. J. Roy. Meteor. Soc.*, **139**, 1132–1161.

Baxter, S. and S. Nigam, 2015: Key role of the North Pacific Oscillation-West Pacific Pattern in generating the extreme 2013/14 North American winter. *J. Climate*, **28**, 8109–8117.

Bond, N. E., M. F. Cronin, H. Freeland, and N. Mantua, 2015: Causes and impacts of the 2014 warm anomaly in the NE Pacific. *Geophys. Res. Lett.*, doi:10.1002/2015GL063306.

Cane, M. A., A. C. Clement, A. Kaplan, Y. Kushnir, D. Pozdnyakov, R. Seager, S. E. Zebiak, and R. Murtugudde, 1997: Twentieth Century sea surface temperature trends. *Science*, **275**, 957–960.

Cayan, D., 1992: Latent and sensible heat flux anomalies over the northern oceans: Driving the sea surface temperature. *J. Phys. Oceanogr.*, **22**, 859–881.

Clement, A. C., R. Seager, M. A. Cane, and S. E. Zebiak, 1996: An ocean dynamical thermostat. *J. Climate*, **9**, 2190–2196.

Davies, H. C., 2015: Weather chains during the 2013/14 winter and their significance for seasonal prediction. *Nature Geo.*, **8**, 833–837.

Funk, C., A. Hoell, and D. Stone, 2014: Examining the contribution of the observed global warming trend to the California droughts of 2012/13 and 2013/14. (In Explaining Extremes of 2013 from a Climate Perspective). *Bull. Amer. Meteor. Soc.*, **95**, S11–S15.

Gill, A. E., 1980: Some simple solutions for heat induced tropical circulation. *Quart. J. Roy. Meteorol. Soc.*, **106**, 447–462.

Harnik, N., R. Seager, N. Naik, M. Cane, and M. Ting, 2010: The role of linear wave refraction in the transient eddy-mean flow response to tropical Pacific SST anomalies. *Quart. J. Roy. Meteor. Soc.*, 2132–2146.

Hartmann, D. L., 2015: Pacific sea surface temperature and the winter of 2014. *Geophys. Res. Lett.*, **42**, doi:10.1002/2015GL063 083.

Herring, S. C., M. P. Hoerling, T. C. Peterson, and P. A. Stott, 2014: Explaining extreme events of 2013 from a climate perspective. *Bull. Amer. Meteor. Soc.*, **95**, S1–S96.

Hoerling, M. P., J. W. Hurrell, and T. Xu, 2001: Tropical origins for recent North Atlantic climate change. *Science*, **292**, 90–92.

Hoskins, B. and K. Karoly, 1981: The steady response of a spherical atmosphere to thermal and orographic forcing. *J. Atmos. Sci.*, **38**, 1179–1196.

Howitt, R. E., J. Medellin-Azuara, D. MacEwan, J. R. Lund, and D. A. Summer, 2014: Economic Analysis of the 2014 Drought for California Agriculture. Tech. rep., Center for Watershed Sciences, University of California, Davis, California, 20 pp.

Huang, B., et al., 2015: Extended reconstructed sea surface temperature version 4 (ERSST.v4). Part I: Upgrades and intercomparisons. *J. Climate*, **28**, 911–930.

Kiehl, J. T., J. J. Hack, G. B. Bonan, B. A. Bovile, D. L. Williamson, and P. J. Rasch, 1998: The National Center for Atmospheric Research Community Climate Model: CCM3. *J. Climate*, **11**, 1131–1149.

Kistler, R., et al., 2001: The NCEP-NCAR 50-year Reanalysis: Monthly means CD-ROM and documentation. *Bull. Am. Meteor. Soc.*, **82**, 247–268.

Lau, N.-C. and M. J. Nath, 1994: A modeling study of the relative roles of tropical and extratropical SST anomalies in the variability of the global atmosphere-ocean system. *J. Climate*, **7**, 1184–1207.

Lau, N.-C. and M. J. Nath, 1996: The role of the 'atmospheric bridge' in linking tropical Pacific ENSO events to extratropical SST anomalies. *J. Climate*, **9**, 2036–2057.

Lee, M., C. Hong, and H. Hsu, 2015: Compounding effects of warm sea surface temperature and reduced sea ice on the extreme circulation over the extratropical North Pacific and North America during the 2013-14 boreal winter. *Geophys. Res. Lett.*, doi:10.1002/2014GL062956.

Palmer, T. N., 2014: Record breaking winters and global climate change. *Science*, **344**, 803–4.

Rayner, N., D. Parker, E. Horton, C. Folland, L. Alexander, D. Rowell, E. Kent, and A. Kaplan, 2003: Global analyses of sea surface temperature, sea ice, and night marine air temperature since the late nineteenth century. *J. Geophys. Res.*, **108**, 10.1029/2002JD002 670.

Sardeshmukh, P. D. and B. J. Hoskins, 1988: The generation of global rotational flow by steady idealized tropical divergence. *J. Atmos. Sci.*, **45**, 1228–1251.

Seager, R., L. Goddard, J. Nakamura, N. Naik, and D. Lee, 2014a: Dynamical causes of the 2010/11 Texas-northern Mexico drought. *J. Hydromet.*, **15**, 39–68.

Seager, R., N. Harnik, Y. Kushnir, W. Robinson, and J. Miller, 2003: Mechanisms of hemispherically symmetric climate variability. *J. Climate*, **16**, 2960–2978.

Seager, R., M. Hoerling, S. Schubert, H. Wang, B. Lyon, A. Kumar, J. Nakamura, and N. Henderson, 2015: Causes of the 2011-14 California drought. *J. Climate*, **28**, 6997–7024.

Seager, R., Y. Kushnir, C. Herweijer, N. Naik, and J. Velez, 2005: Modeling of tropical forcing of persistent droughts and pluvials over western North America: 1856-2000. *J. Climate*, **18**, 4068–4091.

Seager, R., H. Liu, N. Henderson, I. Simpson, C. Kelley, T. Shaw, Y. Kushnir, and M. Ting, 2014b: Causes of increasing aridification of the Mediterranean region in response to rising greenhouse gases. *J. Climate*, **27**, 4655–4676.

Seager, R., N. Naik, W. Baethgen, A. Robertson, Y. Kushnir, J. Nakamura, and S. Jurburg, 2010a: Tropical oceanic causes of interannual to multidecadal precipitation variability in southeast South America over the past century. *J. Climate*, **23**, 5517–5539.

Seager, R., N. Naik, M. A. Cane, N. Harnik, M. Ting, and Y. Kushnir, 2010b: Adjustment of the atmospheric circulation to tropical Pacific SST anomalies: Variability of transient eddy propagation in the Pacific-North America sector. *Quart. J. Roy. Meterorol. Soc.*, **136**, 277–296.

Seager, R., D. Neelin, I. Simpson, H. Liu, N. Henderson, T. Shaw, Y. Kushnir, and M. Ting, 2014c: Dynamical and thermodynamical causes of large-scale changes in the hydrological cycle over North America in response to global warming. *J. Climate*, **27**, 7921–7948.

Seager, R., et al., 2009: Mexican drought: An observational, modeling and tree ring study of variability and climate change. *Atmosfera*, **22**, 1–31.

Swain, D., M. Tsiang, M. Haughen, D. Singh, A. Charland, B. Rajarthan, and N. S. Diffenbaugh, 2014: The extraordinary California drought of 2013/14: Character, context and the role of climate change. (In Explaining Extremes of 2013 from a Climate Perspective). *Bull. Amer. Meteor. Soc..*, **95**, S3–S6.

Trenberth, K., G. W. Branstator, D. Karoly, A. Kumar, N. Lau, and C. Ropelewski, 1998: Progress during TOGA in understanding and modeling global teleconnections associated with tropical sea surface temperature. *J. Geophys. Res.*, **103**, 14 291–14 324.

Wang, H. and S. Schubert, 2014: Causes of the extreme dry conditions over California during early 2013. (In Explaining Extremes of 2013 from a Climate Perspective). *Bull. Amer. Meteor. Soc.*, **95**, S7–S10.

Watson, P. A. G., A. Weisheimer, J. R. Knight, and T. N. Palmer, 2015: The role of the tropical West Pacific in the extreme northern hemisphere winter of 2013/14. *J. Geophys. Res.*, in press.

Williams, A. P., et al., 2015: Correlations between components of the water balance and burned area reveal new insights for predicting forest-fire area in the southwest United States. *Int. J. Wildland Fire*, **24**, 14–26.

Yu, L., X. Jin, and R. Weller, 2008: Multidecade global flux datasets from the Objectively Analyzed Air-sea Fluxes (OAFlux) Project: Latent and sensible heat fluxes, ocean evaporation, and related surface meteorological variables. Tech. rep., Woods Hole Oceanographic Institute OAFlux Project OA-2008-01, 64pp. Woods Hole. Massachusetts., 64 pp.

List of Figures

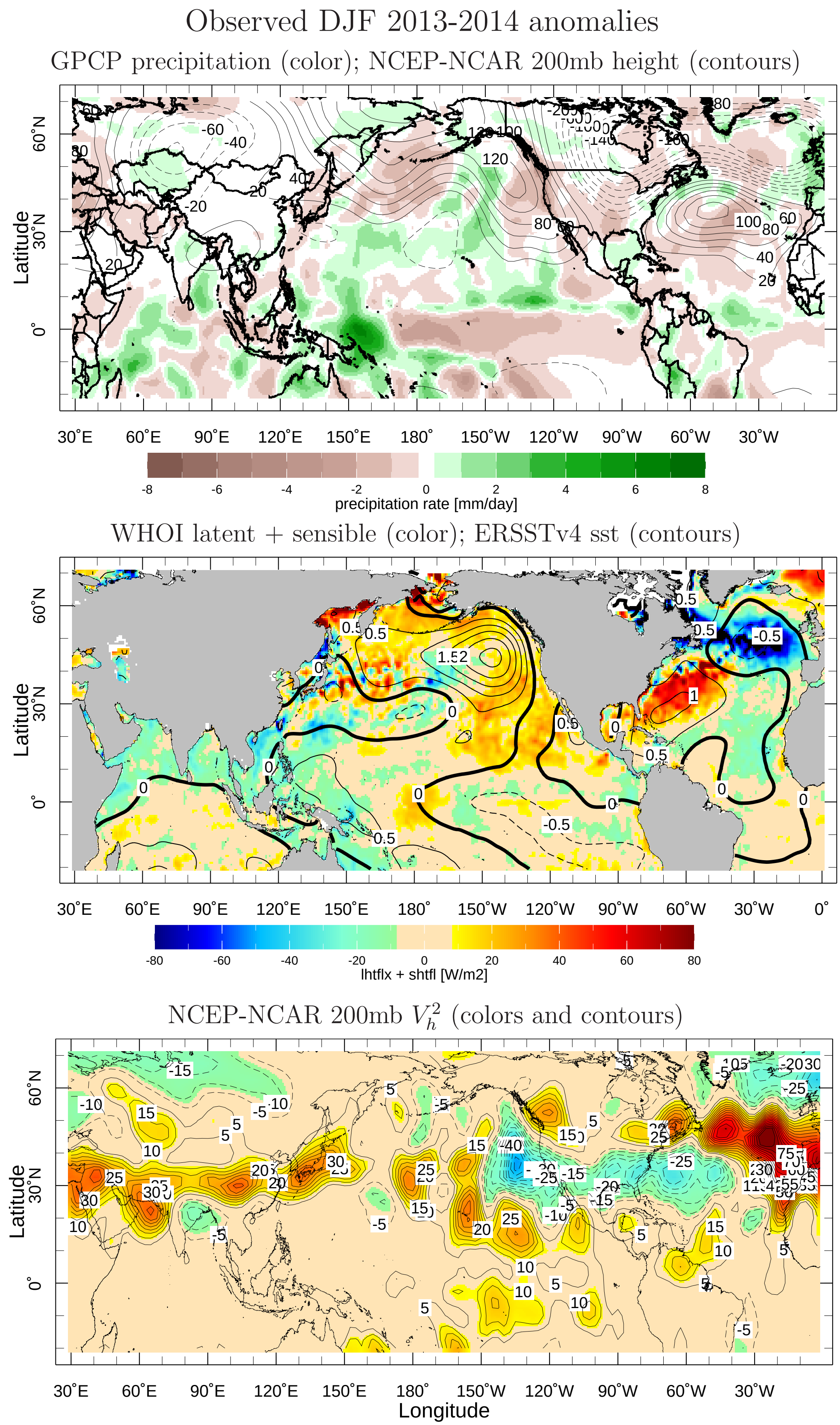

FIG. 1. The observed NCEP-NCAR Reanalysis 200mb height (metres) and GPCP precipitation anomalies (mm/month) (top), ERSSTv4 SST (Kelvin) and OA surface latent plus sensible surface heat flux (W/m^2) anomalies (middle) and NCEP high pass filtered 200mb meridional velocity variance anomaly (bottom) for DJF 2013/14.

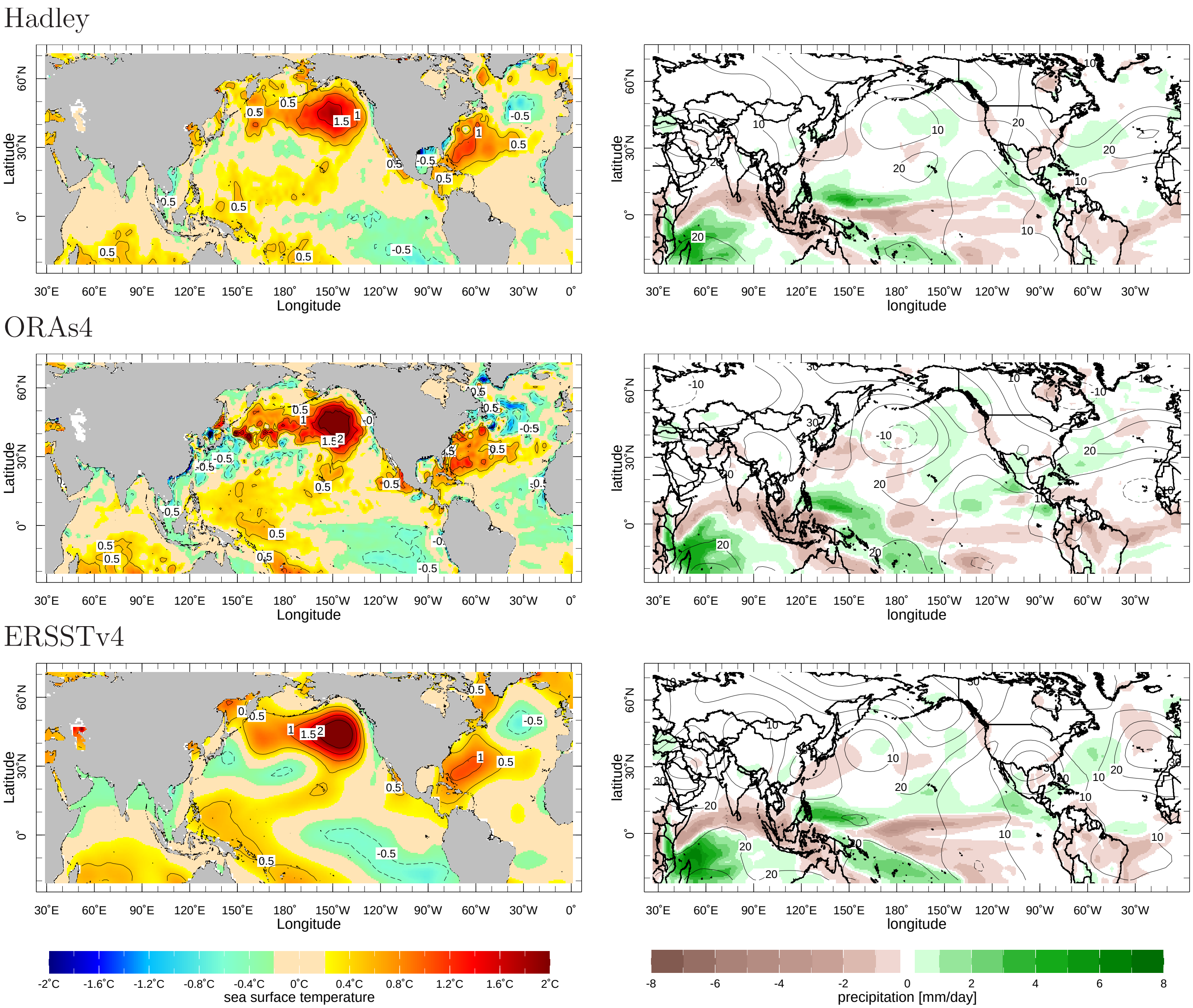

FIG. 2. The observed DJF 2013/14 SST anomalies (left column) from the Hadley (top), ORAs4 (middle) and ERSSTv4 (bottom) data sets and the 100 member ensemble mean 200mb height (contours) and precipitation (colors) response of CCM3 (right column) to these when imposed on the same SST climatology. Units are Kelvin for SST, meters for height and mm/day for precipitation.

SSTA forcing

200mb height response

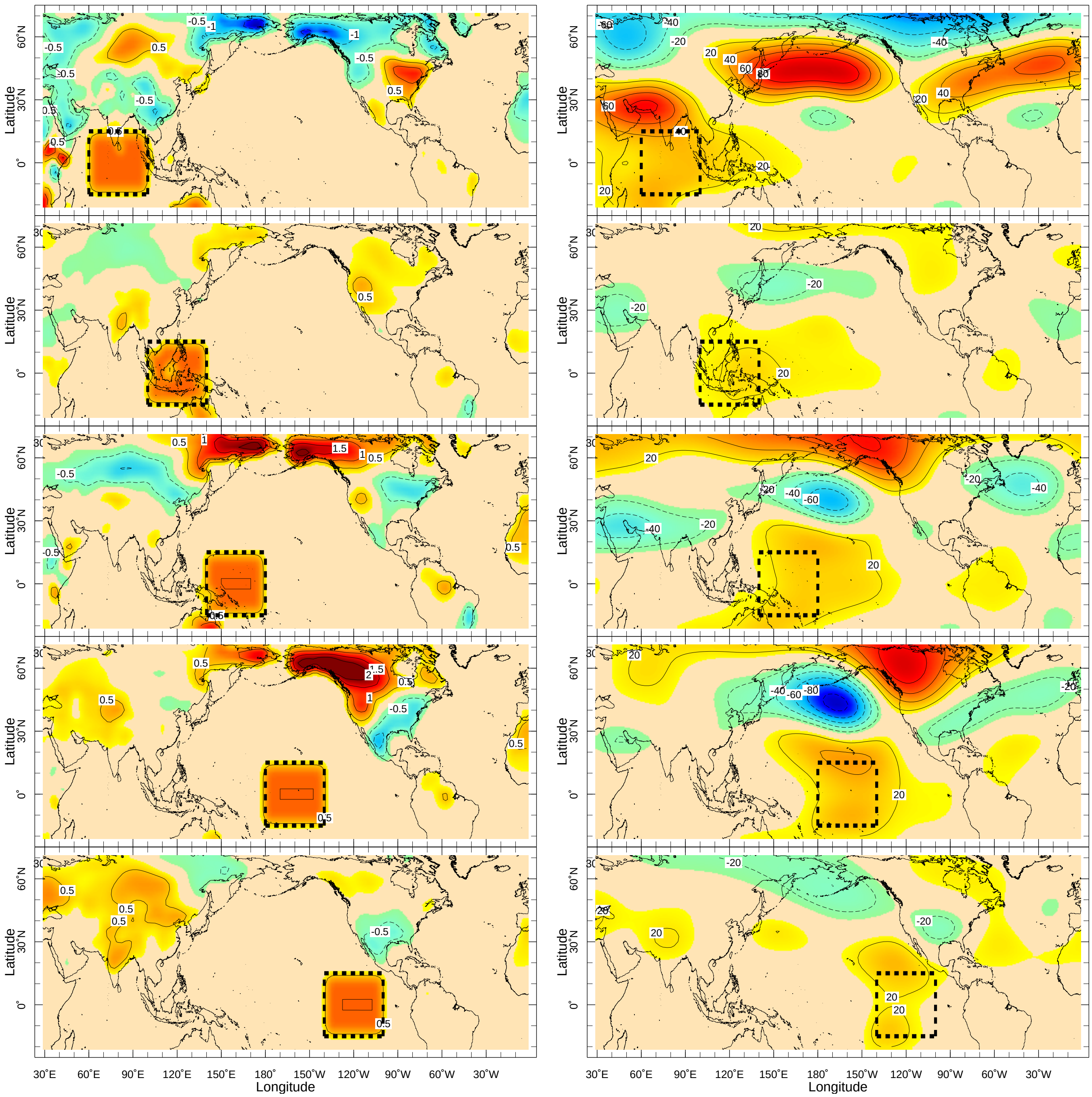

FIG. 3. The imposed "box-SST anomalies" (left column) and the 100 member ensemble mean 200mb height response (right column). The SST anomalies were imposed upon a DJF SST climatology and the average is over days 40-100 of 100 day simulations initiated on December 1st. Units are Kelvin for SST and meters for height.

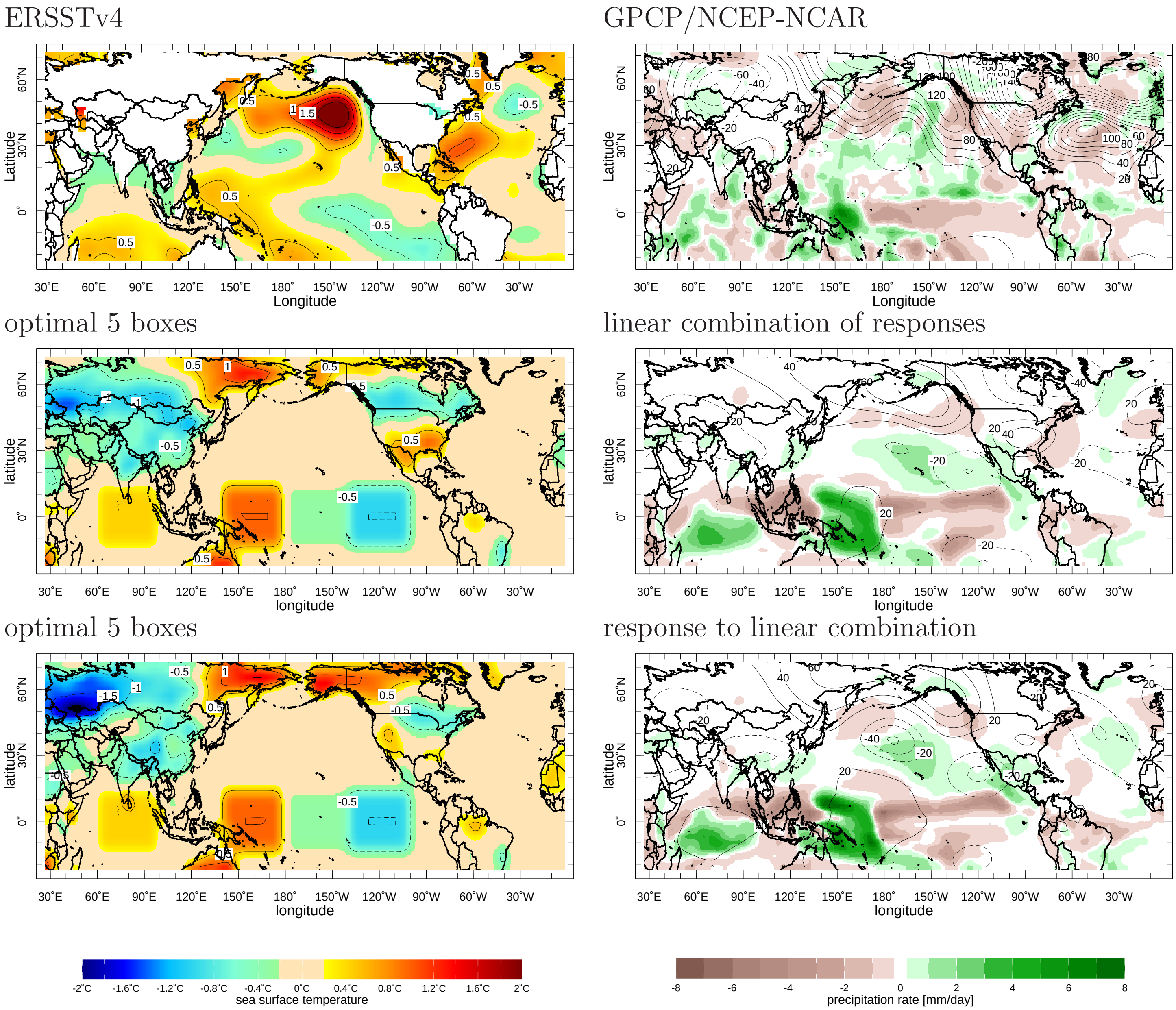

Fig. 4. The ERSSTv4 observed SST anomaly (top left) and the GPCP observed precipitation (colors, top right) and NCEP 200mb height (contours, top right) anomalies for DJF 2013/14. The middle row shows the equivalents constructed by the optimal sum of the "box-SST anomaly" forcing experiments and the bottom row shows the same but for the single ensemble forced by the corresponding constructed SST anomaly. Units are Kelvin for SST, meters for height and mm/day for precipitation.

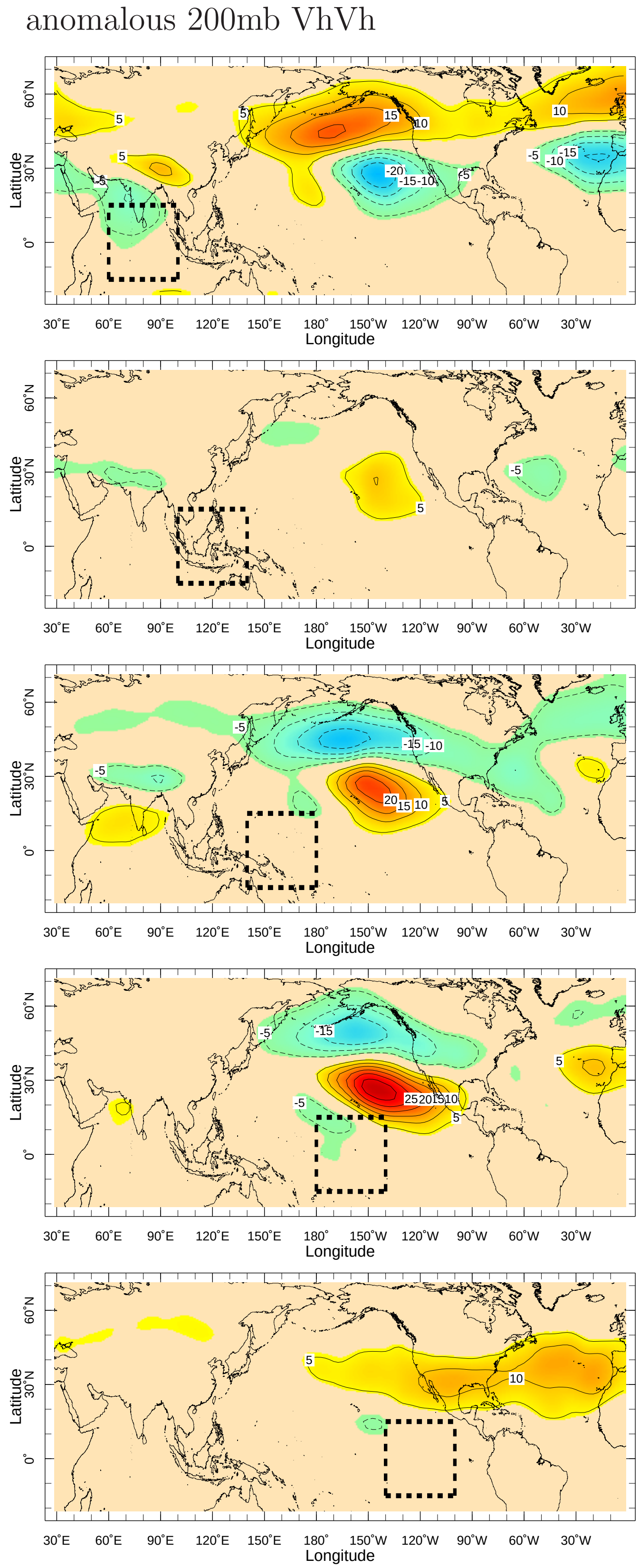

FIG. 5. The high pass filtered 200mb meridional velocity variance for the "box-SST anomalies" experiments. The SST anomalies are shown in Figure 3 and their location indicated here by the boxes. The meridional velocity variances were averaged over days 40-100 of 100 day simulations initiated on December 1st. Units are m^2/s^{-1}.

Response to optimal SST

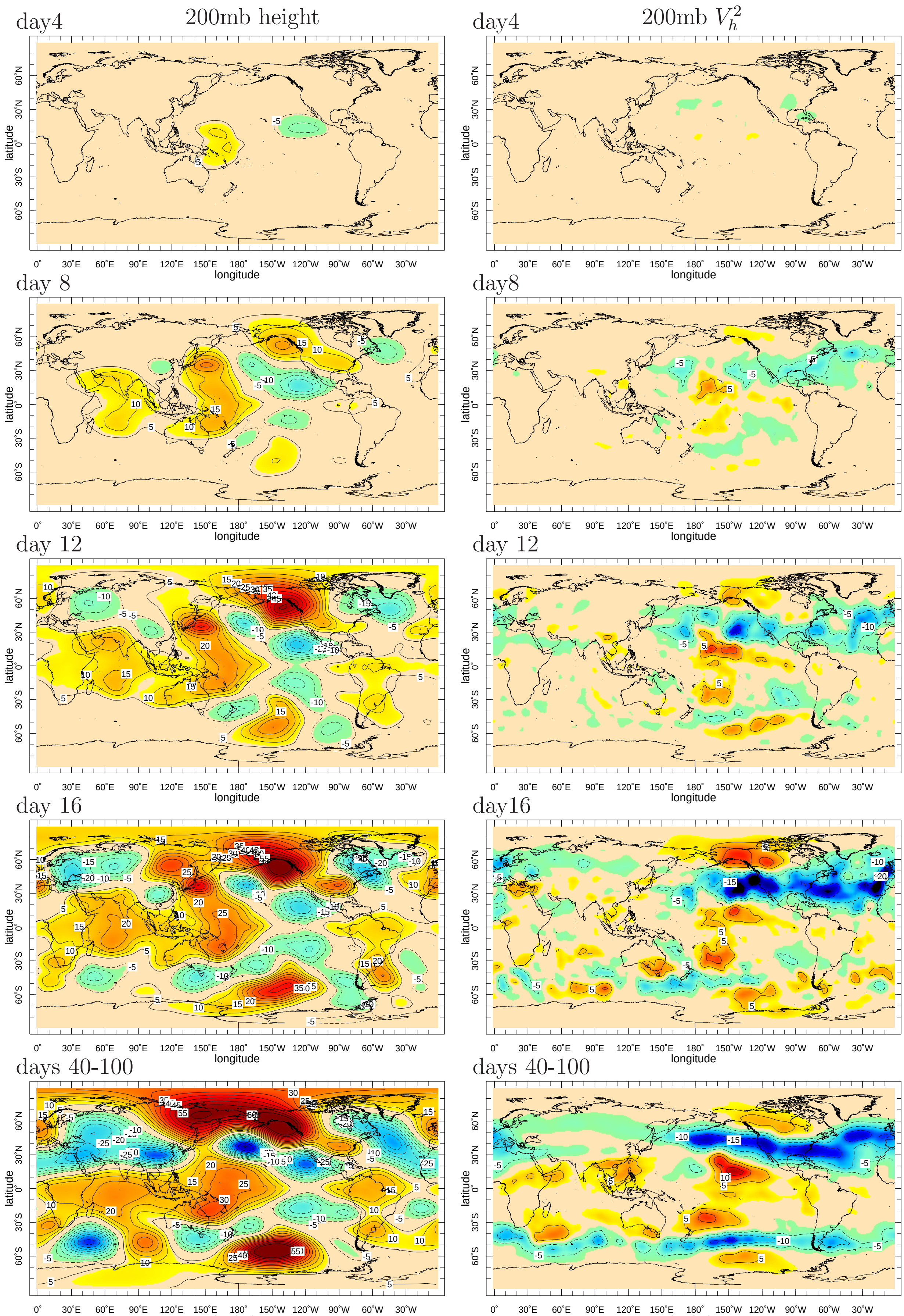

FIG. 6. The 200mb height anomaly (left) and high pass filtered 200mb meridional velocity variance (right) for the optimal SST anomaly experiment as a function of evolution of the SST forced response. Units are m for height and m^2/s^{-2} for velocity variance.

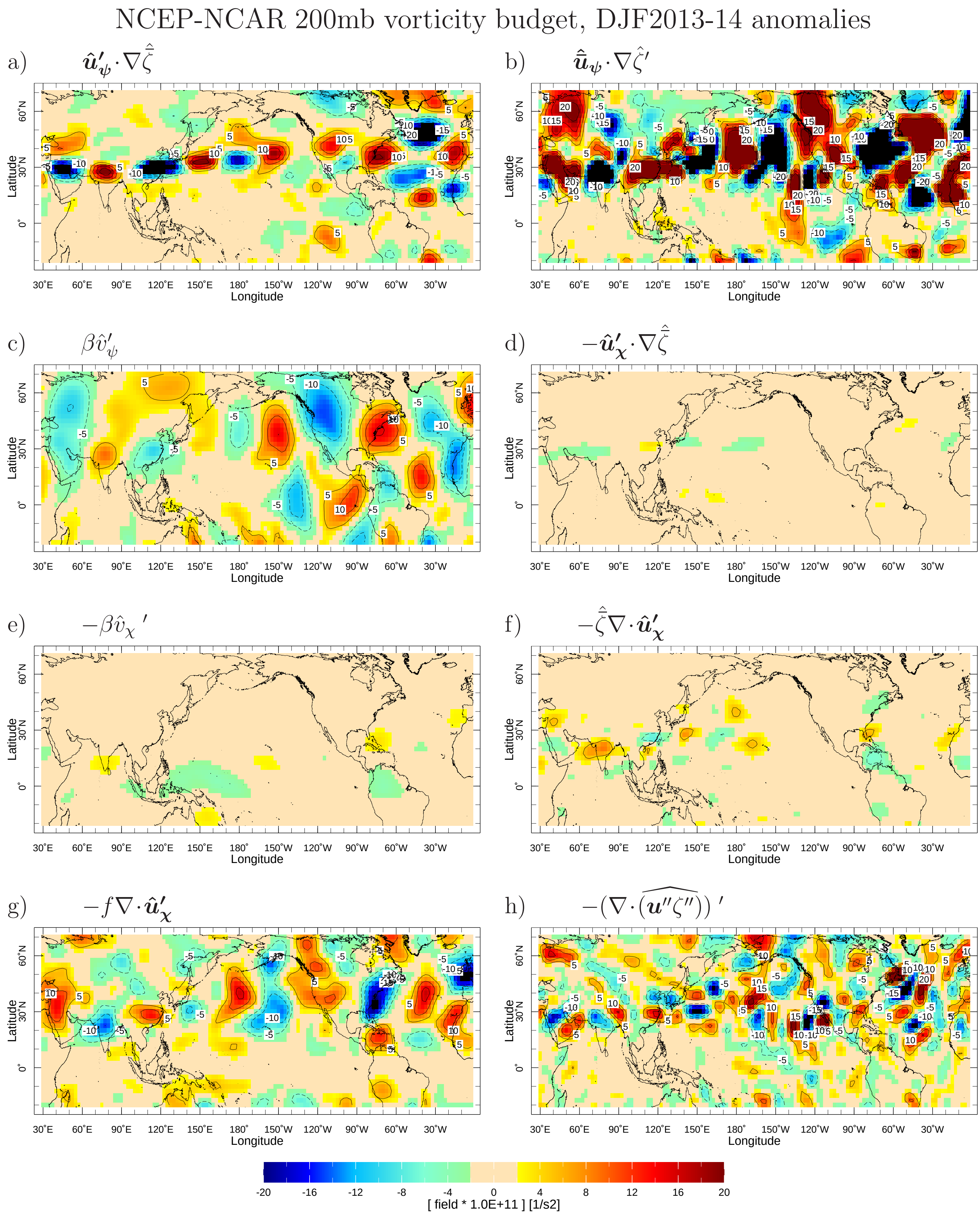

FIG. 7. The terms in the 200mb vorticity budget from the NCEP-NCAR Reanalysis averaged over DJF 2013/14. Units are s^{-2} and terms have been multiplied by 10^6 for plotting purposes.

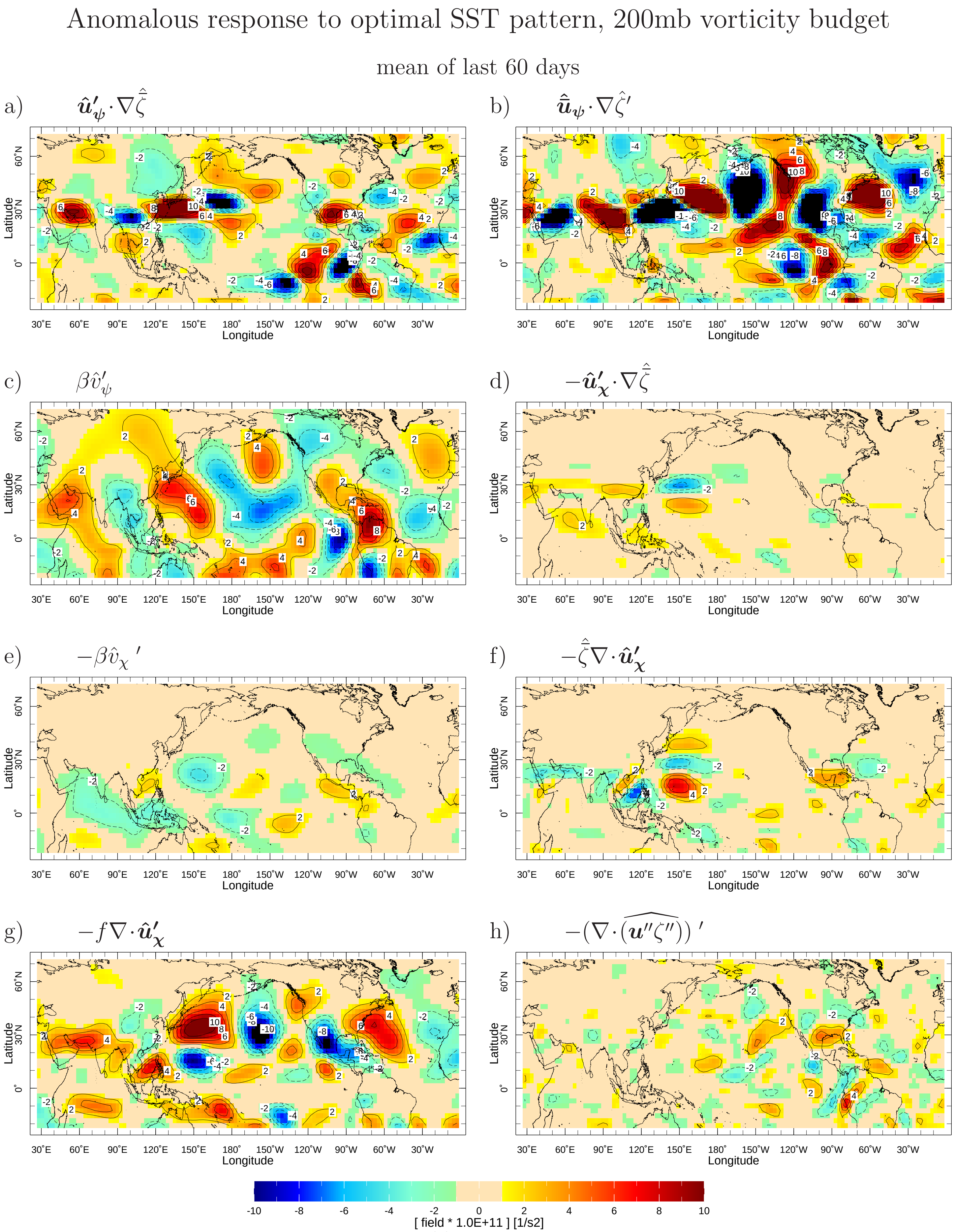

FIG. 8. Same as Figure 7 but for the 100 member ensemble mean of the last 60 days of the model simulations of the response to the optimal SST pattern.

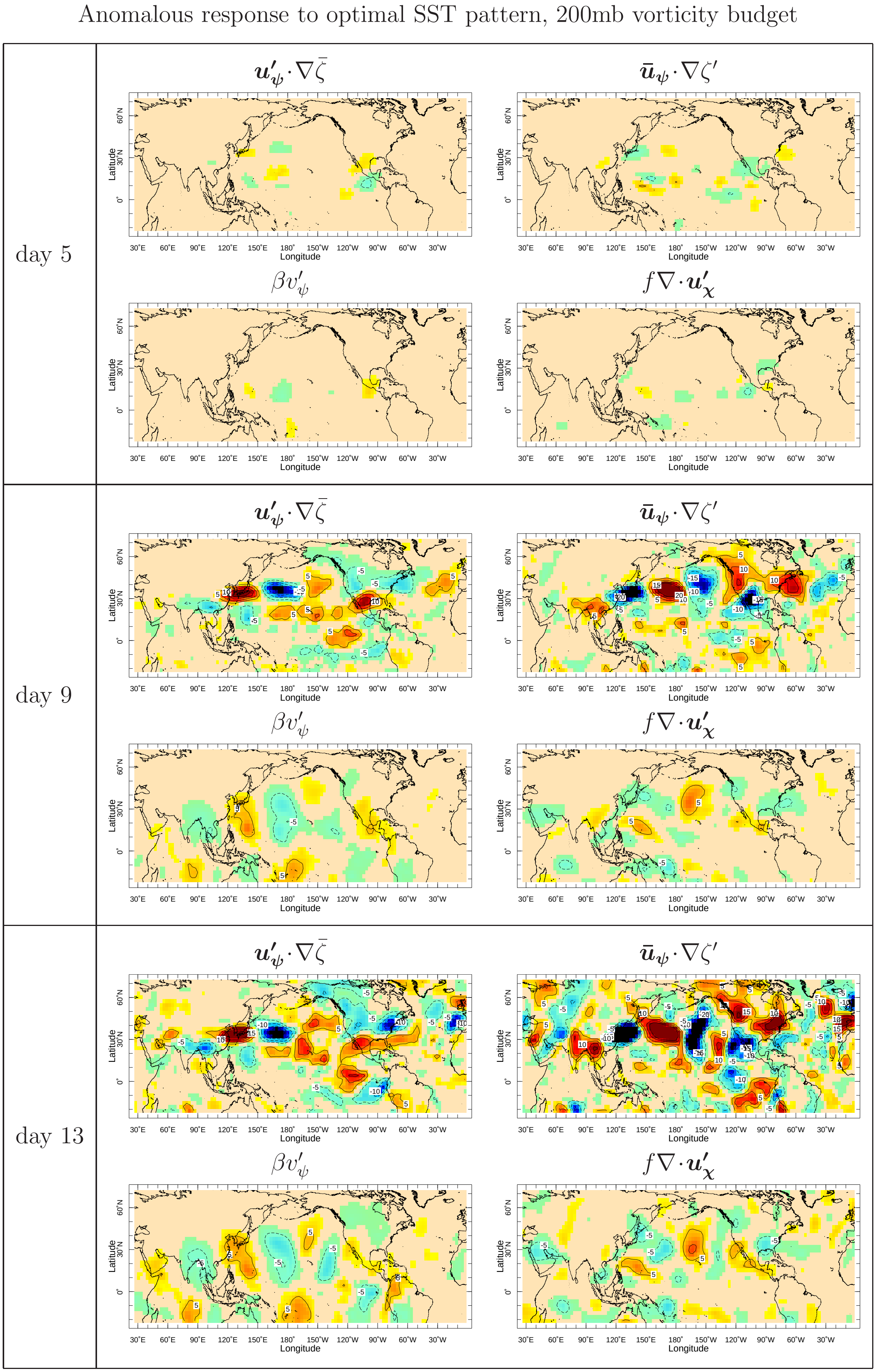

FIG. 9. Day 5 (top), 9 (middle) and 13 (bottom) snapshots of the transient evolution of the leading terms in the vorticity budget of the 100 member ensemble mean of the optimal SST anomaly switch-on experiments. Units are s^{-2} and terms have been multiplied by 10^6 for plotting purposes.

Anomalous response to optimal SST pattern, 200mb vorticity budget

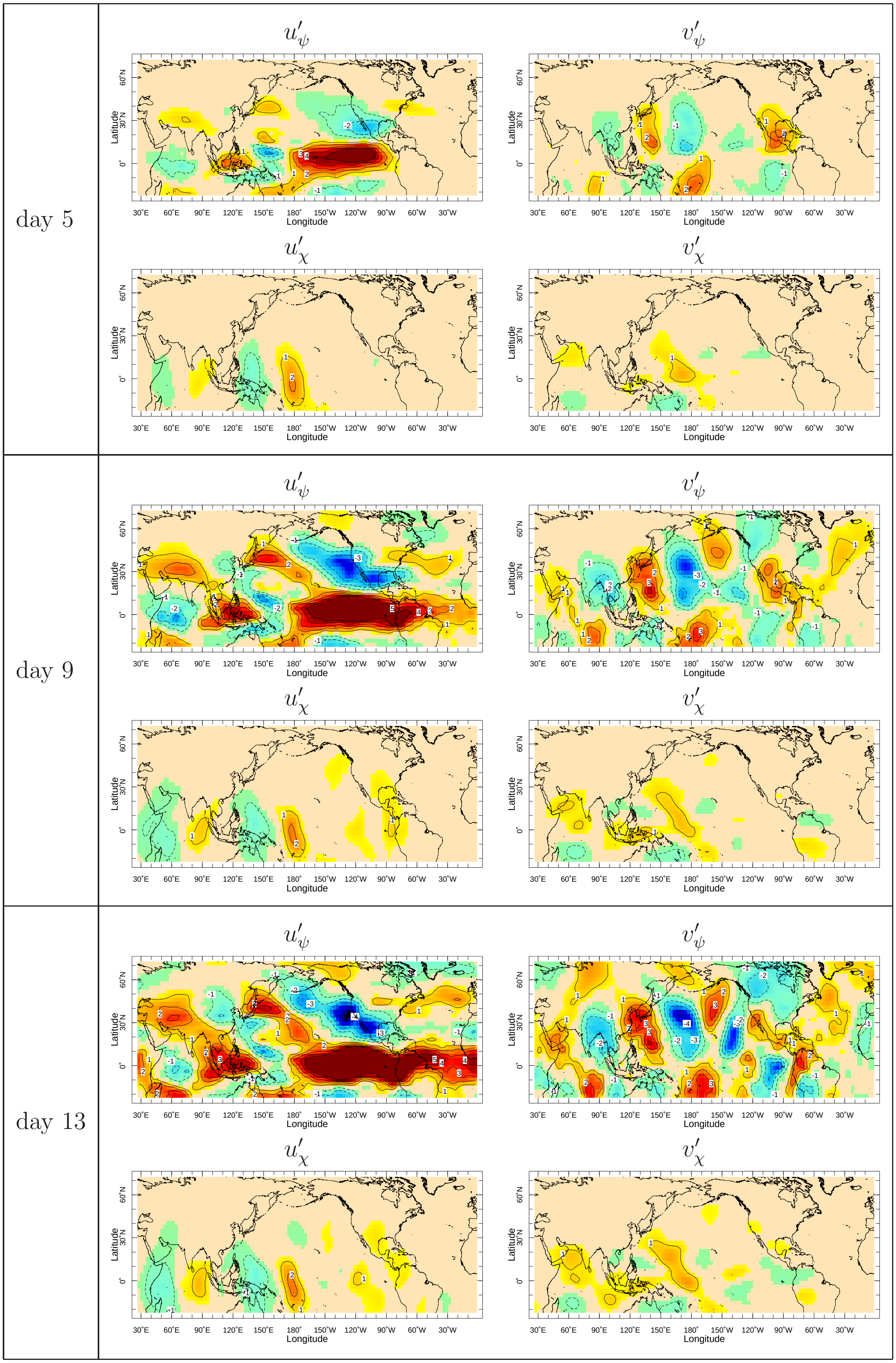

FIG. 10. As for Figure 9 but for the rotational and divergent components of the zonal (left) and meridional (right) flow anomalies. Units are m/s.